

Article

Wireless Power Transfer System with Current-Doubler Rectifier on the Secondary Side—Analysis, Modeling, and Verification

Vladimir Kindl ¹, Martin Zavrel ¹, Miroslav Tyrpekl ¹, Michal Frivaldsky ^{2,*}  and Jakub Skorvaga ²

¹ Faculty of Electrical Engineering, West Bohemian University, 301 00 Pilsen, Czech Republic; vkindl@fel.zcu.cz (V.K.); mzavrel@fel.zcu.cz (M.Z.); mtyrpekl@fel.zcu.cz (M.T.)

² Faculty of Electrical Engineering and Information Technologies, University of Zilina, 010 08 Zilina, Slovakia; jakub.skorvaga@feit.uniza.sk

* Correspondence: michal.frivaldsky@uniza.sk

Abstract: In this paper, the proposal for the performance optimization of the wireless power transfer (WPT) system is given. The solution is based on the alternative configuration of the secondary-side rectifier. It is represented by a diode rectifier with a current doubler. Compared to the bridge rectifier, two diodes are replaced by the inductors. Initially, a system analysis was performed to investigate the electrical behavior and find the most optimal conditions referred to as terms of efficiency performance at nominal power. Due to this requirement, the rectifier inductors must be designed accordingly to meet this condition. The experimental verification was realized as well, while the proposed solution was compared to other common alternatives of the secondary-side rectification. The load sensitivity analysis in terms of efficiency performance was realized as well to observe the system behavior for a wide operation range. From the results, it is seen that the proposed alternative of the secondary-side rectification of the WPT system gives promising results in terms of high operating efficiency.

Keywords: wireless power transfer; diode rectifier; current doubler; equivalent load; compensation; efficiency optimization



Citation: Kindl, V.; Zavrel, M.; Tyrpekl, M.; Frivaldsky, M.; Skorvaga, J. Wireless Power Transfer System with Current-Doubler Rectifier on the Secondary Side—Analysis, Modeling, and Verification. *Electronics* **2023**, *12*, 4818. <https://doi.org/10.3390/electronics12234818>

Academic Editors: Fabio Corti and Spyridon Nikolaidis

Received: 16 October 2023
Revised: 10 November 2023
Accepted: 21 November 2023
Published: 28 November 2023



Copyright: © 2023 by the authors. Licensee MDPI, Basel, Switzerland. This article is an open access article distributed under the terms and conditions of the Creative Commons Attribution (CC BY) license (<https://creativecommons.org/licenses/by/4.0/>).

1. Introduction

The wireless power transfer (WPT) system is recognized as one of the most appropriate technological approaches. WPT has already reached the commercialization stage in inductive pickup systems in manufacturing facilities [1], and it has been used in portable consumer electronics as well as for biomedical applications [2–6] over the last decade. Active research has recently been extended to the static and dynamic charging of electric vehicles [7,8] and medical implants [9,10]. The constant power performance increase in the portable devices wireless chargers creates a significant technical approach for electrical engineers and researchers, which are associated with the effective removal of heat losses outside of the charged accumulator's area. Portable devices have a relatively low charging voltage value and thus a high current value, so together with the value of the parasitic secondary coil series resistance, significant heat losses occur [11–16].

The load resistance of a WPT system should be transformed to the optimum load resistance of the system because the WPT system transfer efficiency is highly dependent on the load impedance. Then, a high-power transfer efficiency for the whole (or most) part of the load range can be achieved. Many studies have been conducted regarding this topic [17–23]. Generally, there are at least four commonly used methods that can realize load resistance transformation [24–26]:

- Using DC-DC converters for altering load impedance;
- Using passive circuits for impedance matching;
- Reconfigurable resonant circuits for impedance matching;
- Using variable operating frequency.

The key will be the nature of the used specific compensation topology for the analyzed WPT system. For example, topology series–series (S-S, compensating for the coils' own inductance), parallel–parallel (P-P), LCC-LCC, LCC-P, and others are characterized by their current output, i.e., they act as a current source. Other topologies, e.g., S-S (compensating for the stray inductance of coils), P-S, S-P, LCC-S, and others, act as a voltage source [27,28]. For a specific type of output, it is most appropriate to use only a compatible current doubler. In principle, two types of current doubler are recognized: a rectifier with coils without magnetic coupling (which is suitable for WPT systems with current output) and a rectifier with magnetically coupled coils (which is suitable for WPT systems with voltage output) [29–31].

EVs with WPT technology usually consider their power batteries to be the energy receiving device. The output power level of the complete WPT system is tied to mutual inductance and equivalent battery resistance. The power sent to the WPT system's secondary side, which employs a bridge rectifier, is insufficient when there is a light load. The system's overall power transmission capacity has been increased through the application of numerous strategies. A novel impedance transfer method based on the combined continuous conduction mode (CCM) and discontinuous conduction mode (DCM) operating out of the buck converter is proposed [32] to track the maximum power transmission. However, the receiving side requires a buck converter, which adds to the cost and installation area of the system. It also requires a switch and three passive elements. The phase difference between the secondary rectifier input voltage and the primary inverter output voltage can be set to 90 to increase the power level, which is in accordance with the auxiliary function of an additional three-coil system [33]. However, to implement the closed-loop control mechanism, wireless communication between the sending and receiving sides is necessary. Unfortunately, the extra communication facilities will result in an increase in system size and expense. Many [34–36] have implemented the frequency adjustment to follow the greatest power transfer as the coupling coefficient moves beyond the critical coupled state. That does, however, primarily address the issue of output power loss under various coupling coefficients. The frequency modification approach is not able to improve the output power reduction caused by the load. However, to achieve optimal coupling efficiency transmission for a specific WPT system, there exists an optimum load R_{opt} [37–39]. The following provides an overview of recent research on tracking maximum efficiency under load fluctuations. To attain optimal efficiency tracking, the variable load R is transferred into R_{opt} via a DC/DC converter that is put on the secondary side. But the DC/DC converter's extra power loss, rising component costs, and large size should raise concerns. To achieve impedance matching, the passive impedance matching network—which consists of the inductor and capacitor network—is positioned in front of the rectifier component. However, there will be the introduction of the unwanted imaginary impedance. By modifying the active rectifier's phase shift angle, the equivalent impedance can be set to the ideal value for attaining the best efficiency. On the other hand, it will become more difficult to control since crossing zero-point detection is required to accurately control the phase-shift angle.

In this paper, focus is given to the performance research of a certain WPT system with a series–series compensation network [40–45] using an alternative secondary-side rectifier topology. The analysis of the impedance ratio is being evaluated in reference to the efficiency of the whole system. More specifically, according to the optimization procedure, we are talking about the possibility of replacing a standard two-way diode (or even synchronous) rectifier in a bridge connection. Using a modified rectifier on the secondary side, which is characterized by a higher impedance conversion, it is naturally possible to establish the conditions for higher achievable efficiency. This approach is favorable for the systems with a low equivalent load; thus, there is no need to consider the use of an additional power converter on the secondary side. The implementation of the proposed rectifier topology increases the voltage at the input of the rectifier, thereby reducing the current through the secondary coil. The proposed solution is analyzed to find the optimal design of the value of inductances to achieve the highest possible operational

efficiency. Experimental verification is given at the end, while the analyzed solution is compared to the common configuration of the WPT system.

2. Analysis of Alternative Secondary-Side Rectifier

Some applications do not require regulation (based on the secondary-side load type). The analyzed system belongs to the case when no WPT system secondary-side regulation is required. For this situation, the common WPT systems use standard bridge diode rectifiers for the secondary-side rectification (Figure 1a), while C block refers to the compensation network, which can be various types.

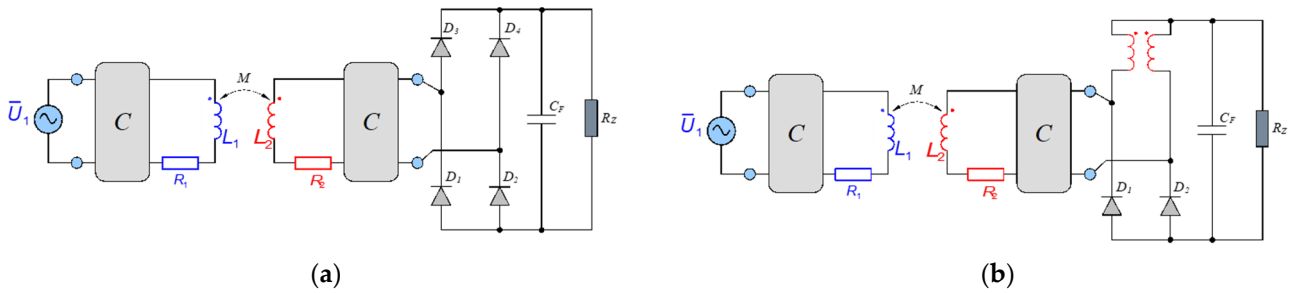


Figure 1. Equivalent schematics of WPT system with standard secondary-side bridge diode rectifier (a). Equivalent schematics of WPT system with modified secondary-side diode rectifier (b).

Because wireless power transfer is currently a matter of supplying power for a wide range of applications, the consideration about the power performance is important regarding proper selection of the optimal secondary-side rectifier topology. Figure 1b shows one possible alternative topology, while upper diodes of the bridge rectifier are replaced by the inductors without any common magnetic coupling. This configuration refers to the current-type rectifier, and its operational behavior is a matter of research within this paper.

2.1. Principle of Operation of Current-Type Rectifier

To explain the operational principle of the WPT system secondary-side current-type rectifier, assumption on the harmonic power supply is made initially (Figure 2), while only the fundamental 1st harmonic is considered. In this way, a certain error is concerned regarding the mathematical model, but this error is not exceptional to prove the operational performance analysis. We are more concerned with a qualitative explanation and not with a precise mathematical description at the beginning. In addition, it would be necessary to consider the specific V-A characteristic of a certain diode. The circuit schematic for the analysis is shown in Figure 3.

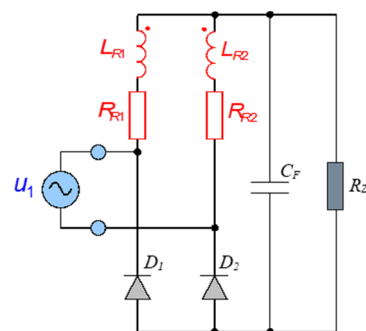


Figure 2. Current-type rectifier with harmonic power supply.

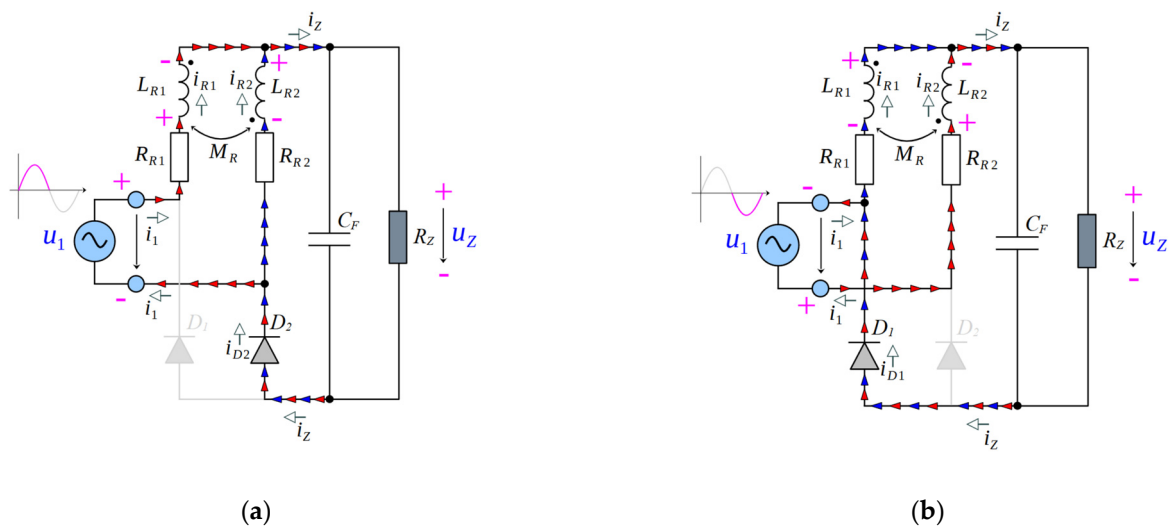


Figure 3. Operation during time Interval A (a). Equivalent operation during time Interval B (b).

Because both inductors are replacing diodes, the same electrical properties are considered for them. Due to the sinusoidal source voltage waveform u_1 of the power supply voltage, the operational cycle of the rectifier is divided into two symmetrical intervals—interval A and interval B (Figure 3).

- INTERVAL A

This interval belongs to the time interval $0 < t < T/2$. The supply voltage is positive, while current is flowing through inductor L_{R1} , parallel load $C_F \parallel R_Z$ and through the diode D_2 , going back to the power supply. At the same time, inductor L_{R2} is supporting this current flow through the sourcing of the energy, which was absorbed during the previous operational cycle.

- INTERVAL B

This interval belongs to the time interval $T/2 < t < T$. The supply voltage has negative polarity, while current is flowing through inductor L_{R2} , parallel load $C_F \parallel R_Z$ and through the diode D_1 , going back to the power supply. At the same time, inductor L_{R1} is supporting this current flow through the sourcing of the energy, which was absorbed during the previous operational cycle.

2.2. Analytical Expression for Optimal Design of Current-Doubler Inductors

A mathematical description of both operational intervals is provided in Equation (1). Using assumption according to the ideal coil of transmitter and receiver of the WPT system ($R_{R1} = R_{R2} = 0$) and considering that the voltage threshold of the diodes is $u_{D1} = u_{D2} = 0$, then Equation (1) can be transformed into a simpler form described by (2).

$$\left(\begin{array}{l} 0 < t < \frac{T}{2} \\ \frac{T}{2} < t < T \end{array} \right) \left\{ \begin{array}{l} \frac{d}{dt} i_{R1} = \frac{1}{L_{R1}} (u_1 - u_Z - u_{D2} - R_{R1} i_{R1}) \\ \frac{d}{dt} i_{R2} = \frac{1}{L_{R2}} (u_Z + u_{D1} + R_{R2} i_{R2}) \\ \frac{d}{dt} i_{R2} = \frac{1}{L_{R2}} (u_1 - u_Z - u_{D1} - R_{R2} i_{R2}) \\ \frac{d}{dt} i_{R1} = \frac{1}{L_{R1}} (u_Z + u_{D2} + R_{R1} i_{R1}) \end{array} \right. \quad (1)$$

$$\begin{aligned} \left(0 < t < \frac{T}{2}\right) & \begin{cases} \frac{d}{dt}i_{R1} = \frac{1}{L_{R1}}(u_1 - u_Z) \\ \frac{d}{dt}i_{R2} = \frac{u_Z}{L_{R2}} \end{cases} \\ \left(\frac{T}{2} < t < T\right) & \begin{cases} \frac{d}{dt}i_{R2} = \frac{1}{L_{R2}}(u_1 - u_Z) \\ \frac{d}{dt}i_{R1} = \frac{u_Z}{L_{R1}} \end{cases} \end{aligned} \tag{2}$$

If $L_{R1} = L_{R2}$ is valid, then from (2), it is possible to find out similarity regarding expressions for currents i_{R1} and i_{R2} . The difference reflected within the signs is related to the mutual phase shift, which is equal to 180° . Exact expressions for time-dependent currents are gained through the integration of (2), while Equations (3) and (4) have the following form:

$$\begin{aligned} & \left(0 < t < \frac{T}{2}\right) \\ i_{R1}(t) &= i_{R1}(0) + \frac{U_m}{\omega L_{R1}}(1 - \cos(\omega t)) - \frac{u_Z}{L_{R1}}t ; U_m = \sqrt{2}u_1 \\ & \left(\frac{T}{2} < t < T\right) \end{aligned} \tag{3}$$

$$i_{R1}(t) = i_{R1}\left(\frac{T}{2}\right) + \frac{u_Z}{L_{R1}}\left(\frac{T}{2} - t\right)$$

$$\begin{aligned} & \left(0 < t < \frac{T}{2}\right) \\ i_{R2}(t) &= i_{R2}(0) - \frac{u_Z}{L_{R2}}t \\ & \left(\frac{T}{2} < t < T\right) \end{aligned} \tag{4}$$

$$i_{R2}(t) = i_{R2}\left(\frac{T}{2}\right) + \frac{U_m}{\omega L_{R2}}(1 + \cos(\omega t)) + \frac{u_Z}{L_{R2}}\left(\frac{T}{2} - t\right)$$

By implementing the condition $L_{R1} = L_{R2} = L_{R0}$, Equations (5) and (6) are obtained:

$$\begin{aligned} & \left(0 < t < \frac{T}{2}\right) \\ i_{R1}(t) &= i_{R1}(0) + \frac{U_m}{\omega L_{R0}}(1 - \cos(\omega t)) - \frac{u_Z}{L_{R0}}t \\ & \left(\frac{T}{2} < t < T\right) \end{aligned} \tag{5}$$

$$i_{R1}(t) = i_{R1}\left(\frac{T}{2}\right) + \frac{u_Z}{L_{R0}}\left(\frac{T}{2} - t\right)$$

$$\begin{aligned} & \left(0 < t < \frac{T}{2}\right) \\ i_{R2}(t) &= i_{R2}(0) - \frac{u_Z}{L_{R0}}t \\ & \left(\frac{T}{2} < t < T\right) \end{aligned} \tag{6}$$

$$i_{R2}(t) = i_{R2}\left(\frac{T}{2}\right) + \frac{U_m}{\omega L_{R0}}(1 + \cos(\omega t)) + \frac{u_Z}{L_{R0}}\left(\frac{T}{2} - t\right)$$

Because both i_{R1} and i_{R2} have periodic character, Equation (7) can be defined:

$$\begin{aligned} i_{R2}(0) &= i_{R1}\left(\frac{T}{2}\right) \\ i_{R2}\left(\frac{T}{2}\right) &= i_{R1}(0) \end{aligned} \tag{7}$$

Considering (7), it is possible to determine average values (8) of both investigated currents I_{R1} and I_{R2} :

$$\begin{aligned} I_{R1} &= \frac{1}{T} \left[\int_0^{\frac{T}{2}} \left(i_{R1}(0) + \frac{U_m}{\omega L_{R0}} (1 - \cos(\omega t)) - \frac{u_Z}{L_{R0}} t \right) dt \right. \\ &\quad \left. + \int_{\frac{T}{2}}^T \left(i_{R1}(0) + \frac{U_m}{\omega L_{R0}} \left(1 - \cos\left(\omega \frac{T}{2}\right) \right) - \frac{u_Z}{L_{R0}} \frac{T}{2} + \frac{u_Z}{L_{R0}} \left(\frac{T}{2} - t \right) \right) dt \right] \\ &= i_{R1}(0) + \frac{3}{2} \frac{U_m}{\omega L_{R0}} - \frac{T}{2} \frac{u_Z}{L_{R0}} \\ I_{R2} &= \frac{1}{T} \left[\int_0^{\frac{T}{2}} \left(i_{R1}(0) + \frac{U_m}{\omega L_{R0}} (1 - \cos(\omega t)) - \frac{u_Z}{L_{R0}} \frac{T}{2} - \frac{u_Z}{L_{R0}} t \right) dt \right. \\ &\quad \left. + \int_{\frac{T}{2}}^T \left(i_{R1}(0) + \frac{U_m}{\omega L_{R0}} \left(1 + \cos\left(\omega \frac{T}{2}\right) \right) + \frac{u_Z}{L_{R0}} \left(\frac{T}{2} - t \right) \right) dt \right] \\ &= i_{R1}(0) + \frac{3}{2} \frac{U_m}{\omega L_{R0}} - \frac{T}{2} \frac{u_Z}{L_{R0}} \end{aligned} \tag{8}$$

Equation (8) just confirms the above-mentioned assumption about the same waveforms of both currents except for their phase shift. Typical waveforms can be seen in Figure 4.

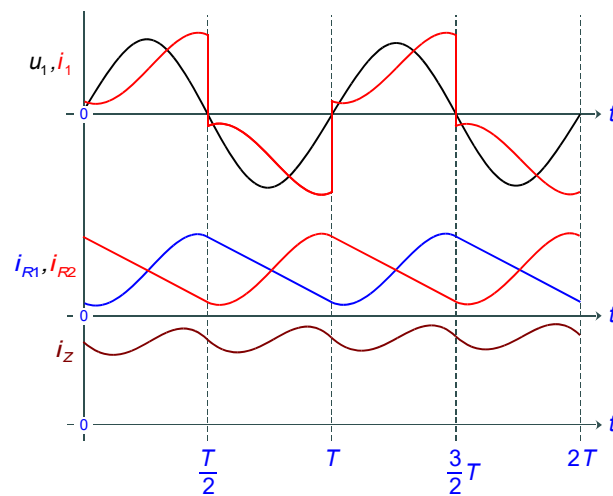


Figure 4. Typical time waveforms of rectifier with current doubler.

At this point, the determination of the voltage and current ratio of the circuit will be determined, while the constant load voltage value is considered. Because of the current

periodicity, the condition $i_{R1}(T) = i_{R1}(0)$ is valid. Then, using (5), Equation (9) can be found:

$$i_{R1}\left(\frac{T}{2}\right) + \frac{U_Z}{L_{R0}}\left(\frac{T}{2} - T\right) = i_{R1}(0) \tag{9}$$

To find required relations, it is important to substitute $i_{R1}(T/2)$, while Equation (10) is then found as:

$$i_{R1}(0) + \frac{U_m}{\omega L_{R0}}\left(1 - \cos\left(\omega \frac{T}{2}\right)\right) - \frac{U_Z}{L_{R0}}\frac{T}{2} + \frac{U_Z}{L_{R0}}\left(\frac{T}{2} - -T\right) = i_{R1}(0) \tag{10}$$

From (10), the unknown ratio can be found as follows:

$$\begin{aligned} i_{R1}(0) + 2\frac{U_m}{\omega L_{R0}} - \frac{U_Z}{L_{R0}}\frac{T}{2} + \frac{U_Z}{L_{R0}}\left(\frac{T}{2} - T\right) &= i_{R1}(0) \\ \downarrow \\ 2\frac{U_m}{2\pi f L_{R0}} &= \frac{U_Z}{L_{R0}}\frac{1}{f} \\ \downarrow \\ \frac{\sqrt{2}}{\pi}U_1 &= U_Z \end{aligned} \tag{11}$$

Taking into account the invariance of powers in the ideal power transfer case, i.e., $U_1I_1 = U_ZI_Z$ at a fully resonant state, the current ration can be directly described by (12)

$$\frac{\pi}{\sqrt{2}}I_1 = I_Z \tag{12}$$

Now, the description is generally valid; nevertheless, in real applications, slightly non-resonant states are neglected with tolerable error.

For completeness, the value of $i_{R1(0)}$ would be determined, which is required for the calculation of all system currents. The procedure is made under the assumption that the load current is given by the instantaneous sum of the currents $i_{R1(t)}$ and $i_{R2(t)}$. The formula is described by (13).

$$I_Z = \frac{U_Z}{R_Z} = I_{R1} + I_{R2} = 2\left(i_{R1}(0) + \frac{3}{2}\frac{U_m}{\omega L_{R0}} - \frac{T}{2}\frac{U_Z}{L_{R0}}\right) \tag{13}$$

By solving (13), Equation (14) is found:

$$i_{R1}(0) = \frac{U_Z}{2R_Z} - \frac{U_Z\pi}{2\omega L_{R0}} \tag{14}$$

The principle of the rectifier was explained in Figures 4 and 5 and through Equation (1). However, based on previous assumptions, Formula (15) can be defined.

$$\begin{aligned} &\left(0 < t < \frac{T}{2}\right) \\ i_1(t) = i_{R1}(t) &= i_{R1}(0) + \frac{U_m}{\omega L_{R0}}(1 - \cos(\omega t)) - \frac{U_Z}{L_{R0}}t \\ &\left(\frac{T}{2} < t < T\right) \\ i_1(t) = -i_{R2}(t) &= -\left[i_{R2}\left(\frac{T}{2}\right) + \frac{U_m}{\omega L_{R0}}(1 + \cos(\omega t)) + \frac{U_Z}{L_{R0}}\left(\frac{T}{2} - t\right)\right]; \quad i_{R2}\left(\frac{T}{2}\right) = i_{R1}(0) \end{aligned} \tag{15}$$

Therefore, it can be seen that the current has the same shape (only with the opposite sign) in both the positive and negative half-waves of the input voltage. In this particular case, it is a quasi-rectangular waveform, which is based on the assumption of a sinusoidal power supply. Considering the connection of the rectifier to a WPT circuit with a current

output, the current and voltage have a harmonic time dependency. For this reason, the logical step is to perform a harmonic decomposition of the relations defined by (14) using the Fourier transform and thereby obtain its fundamental harmonic (16). The parameters a_0 , a_1 and b_1 , used in (16), denote the Fourier coefficients.

$$i_1(t) \approx \frac{a_0}{2} + a_1 \cos(\omega t) + b_1 \sin(\omega t) \tag{16}$$

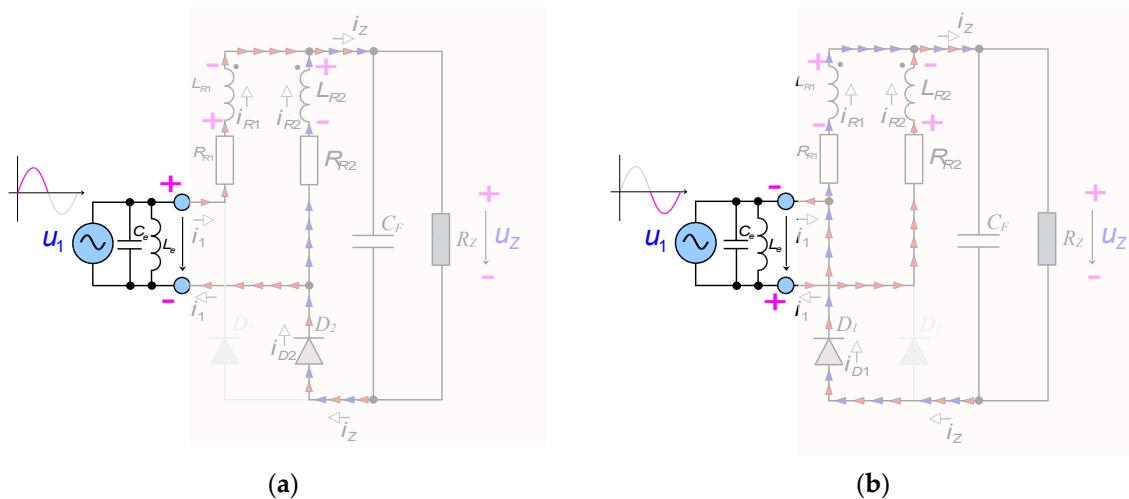


Figure 5. Operation during time Interval A including compensation network (a). Equivalent operation during time Interval B including compensation network (b).

By the substitution of (11) into (15), we obtain the formula for the total waveform of the input current (17).

$$i_1(t) = \frac{U_Z}{2R_Z} - \frac{U_Z}{2\omega L_{R0}} + \frac{U_Z \pi}{\omega L_{R0}} (1 - \cos(\omega t)) - \frac{U_Z}{L_{R0}} t \tag{17}$$

$$i_1(t) = \frac{U_Z}{2R_Z} - \frac{U_m \pi}{2\omega L_{R0}} + \frac{U_Z \pi}{\omega L_{R0}} (1 + \cos(\omega t)) + \frac{U_Z}{L_{R0}} \left(\frac{T}{2} - t \right)$$

The Fourier coefficients are determined by Equation (18):

$$a_0 = \frac{2}{T} \int_0^T i_1(t) dt = 0$$

$$a_1 = \frac{2}{T} \int_0^T i_1(t) \cos(\omega t) dt = - \left(\frac{\pi^2 - 4}{\pi^2} \right) \frac{U_Z \pi}{\omega L_{R0}} \tag{18}$$

$$b_1 = \frac{2}{T} \int_0^T i_1(t) \sin(\omega t) dt = \frac{2U_Z}{\pi R_Z} + \left(\frac{\pi - 1}{\pi} \right) \frac{2U_Z}{\omega L_{R0} R_Z}$$

Then, the fundamental harmonic of the current is described by (19).

$$i_1(t) \approx \left[\frac{2U_Z}{\pi R_Z} + \left(\frac{\pi - 1}{\pi} \right) \frac{2U_Z}{\omega L_{R0} R_Z} \right] \sin(\omega t) - \left(\frac{\pi^2 - 4}{\pi^2} \right) \frac{U_Z \pi}{\omega L_{R0}} \cos(\omega t) \tag{19}$$

Current i_1 consists of two harmonic waves: the first one corresponds to the sine function, while the second one corresponds to the minus cosine function. Since the voltage u_1 varies according to the sine function, the first current component is in phase with the

voltage, and the second one lags by 90°. Regarding the theory of first-harmonic analysis, we can declare the second component as an imaginary part of the net current.

Recall that $u_1 = U_m \sin(\omega t)$ is valid; then, using Equation (20), it is possible to find out that two currents are phase shifted by 90°, while the first of them has a pure ohmic character, whereby the second one has an imaginary character.

$$\frac{u_1}{i_1} \approx \frac{U_1}{I_1} \approx \frac{\frac{\pi U_Z}{\sqrt{2}} \sin(\omega t)}{\left[\frac{2}{\sqrt{2}} \frac{U_Z}{\pi R_Z} + \left(\frac{\pi-1}{\pi} \right) \frac{2}{\sqrt{2}} \frac{U_Z}{\omega L_{R0} R_Z} \right] \sin(\omega t) - \left(\frac{\pi^2-4}{\pi^2} \right) \frac{U_Z \pi}{\omega L_{R0} \sqrt{2}} \cos(\omega t)} \tag{20}$$

With respect to the supply voltage, the rectifier behaves like a load composed of parallel resistance and inductance. This inductance will negatively affect the power factor of the rectifier and must be dealt with. So, from Equation (20), we determine the imaginary component of impedance (21),

$$\Im \left\{ \frac{U_1}{I_1} \right\} \approx \frac{\frac{\pi U_Z}{\sqrt{2}}}{\left(\frac{\pi^2-4}{\pi^2} \right) \frac{U_Z \pi}{\omega L_{R0} \sqrt{2}}} = \left(\frac{\pi^2}{\pi^2-4} \right) \omega L_{R0} \Rightarrow L_e = \left(\frac{\pi^2}{\pi^2-4} \right) L_{R0} \tag{21}$$

which (among other things) shows the way of reflected L_{R0} onto the input terminals of the rectifier, i.e., the converted inductance L_e . Its influence can be fully compensated by an additional capacitor C_e (22) connected in parallel to the input terminals of the rectifier (see Figure 5).

$$C_e = \frac{1}{2\omega^2 L_e} = \frac{1}{\omega^2 \left(\frac{\pi^2}{\pi^2-4} \right) L_{R0}} \tag{22}$$

This unity power factor ensures that both the input voltage and the drawn current are in phase.

The last step is to determine the inductance L_{R0} value. Equation (2) should be used as the initial condition, while in combination with Equation (11) and Equation (12), the consideration on the harmonic waveforms gives the formula for inductance (23).

$$L_{R0} = \frac{R_Z}{\omega} \left(\frac{\pi-1}{\pi} \right) \tag{23}$$

Looking at (22) shows that the expression represents a simple relationship, but the design challenge is represented by the load value dependency. Because of this relationship, the analyzed solution of the WPT system would be well suited for the systems with constant power requirements.

3. Comparison of WPT System Performance for Bridge Diode Rectifier and Proposed Circuit Modification

Experimental verification was provided for a quantitative comparison of the analyzed secondary-side rectifier alternative, while the most common compensation network for the transmitting and receiving side was used (series-series compensation) [27–29]. The analyzed system is compared to the WPT system using a standard bridge-diode rectifier. The input to output parameters are listed in Table 1. U_{1amp} refers to the input voltage amplitude, U_{2batt} is the secondary-side voltage required by the load, f_{sw} is the primary-side converter switching, P_Z is the output power, k is the coupling coefficient and p is the ratio between the primary and secondary side.

Table 1. Input to output nominal parameters of experimental test.

U_{1amp} (V)	U_{2batt} (V)	f_{sw} (kHz)	P_Z (W)	k (-)	p (-)
$\frac{4}{\pi} 55$	18	577	200	0.5	1

Table 2 indicates the values of the circuit parameters, while L_1 and L_2 are the values of inductances of the primary and secondary coil, C_1 and C_2 are the values of compensation capacitances, R_1 and R_2 are parasitic resistances of primary and secondary coils, and R_Z is the value of the load resistance.

Table 2. Values of the circuit components of investigated WPT system.

$L_1 = L_2$ (μH)	$C_1 = C_2$ (nF)	$R_1 = R_2$ (m Ω)	R_Z (Ω)
5.5	142.12	90×10^{-3}	1.62

In order to verify the electrical behavior of both alternatives, circuit simulation in the time domain was realized considering the operation reflecting the optimal value of the load. The simulation models are shown in Figure 6, while the primary-side inverter is represented by voltage-source replacement.

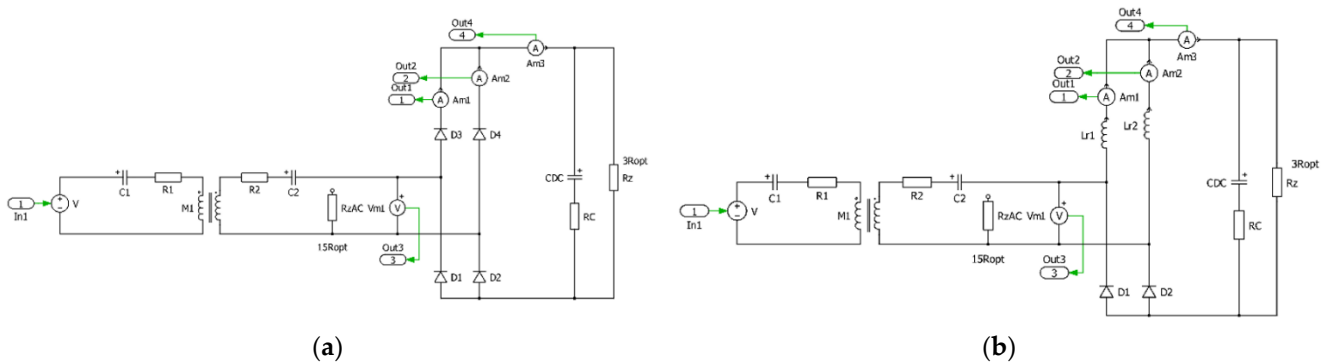


Figure 6. Circuit diagram of simulation model for WPT system with bridge-diode rectifier (a) and proposed alternative (b).

Our main focus was concentrated on the time waveforms of the currents, which flow through individual legs of the rectifier (I_a , I_b), the load current, I_{load} , and the secondary-side voltage induced on the receiving coil U_2 . Figure 7a shows time waveforms of the mentioned circuit variables for the bridge-diode rectifier, while Figure 7b represents the situation for the current doubler rectifier.

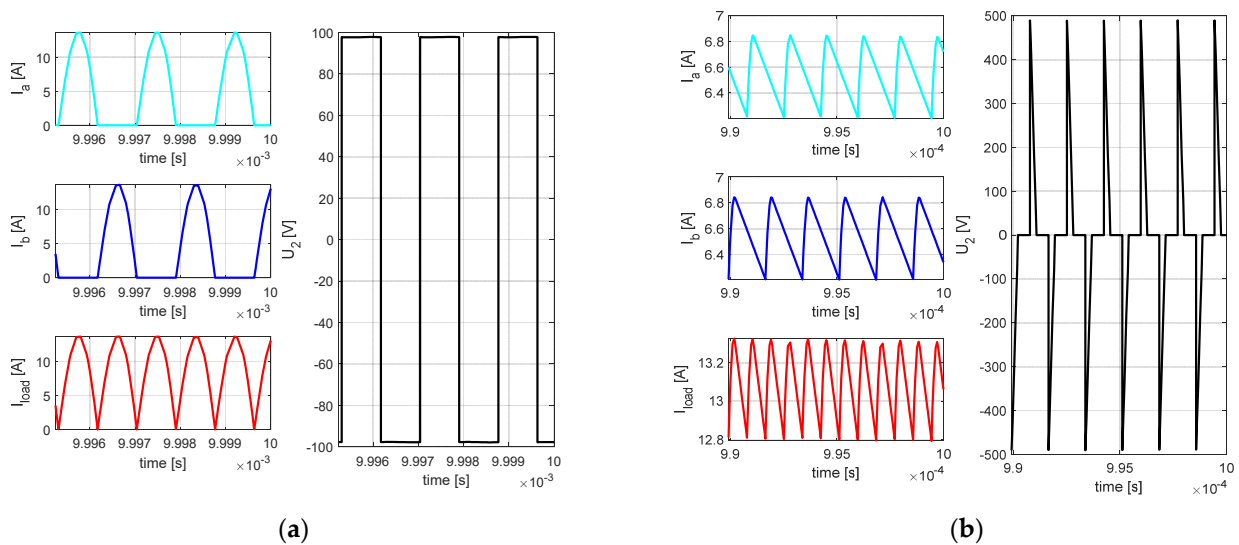


Figure 7. Time waveforms of selected electrical variables for bridge-diode rectifier (a) and time waveforms of selected electrical variables for current-doubler rectifier (b).

Regarding the results of the WPT system with a bridge-diode rectifier, the currents I_a and I_b are forming the load current I_{load} . The secondary-side voltage has a rectangular shape corresponding to the operation of the voltage diode rectifier.

The waveforms of I_a and I_b of the current-doubler rectifier are mutually shifted by 90° . I_{load} is the sum of both of these leg currents. The ratio of the current ripple is affected by the value of inductors, while referring to the triangle shape of the currents reflects into a highly distorted shape of secondary-side voltage U_2 . This is valid also for the primary-side coil. During diode commutation, an extreme rise of the voltage is visible followed by its gradual decrease during the I_{load} rise. After this transient period, the U_2 voltage is practically zero (Figure 8). By reduction in the value of inductance of the current-doubler rectifier, it is possible to reduce the maximum values of voltage U_2 . However, the efficiency and power transmission will be reduced as well.

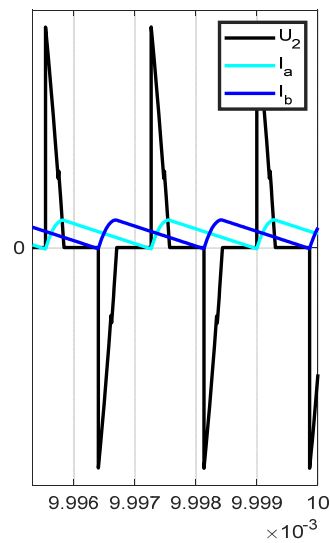


Figure 8. Time waveform of selected electrical variables for current-doubler rectifier.

4. Experimental Verification

Figure 9a shows the block diagram of the system setup during experimental verifications, while Figure 9b shows the physical prototype with laboratory equipment of the analyzed WPT system.

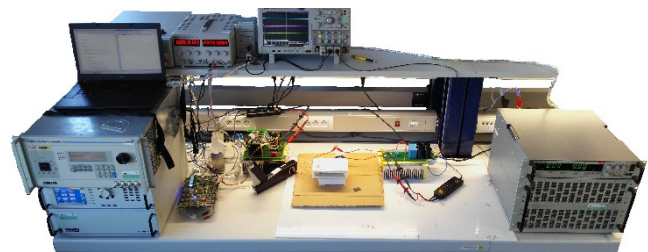
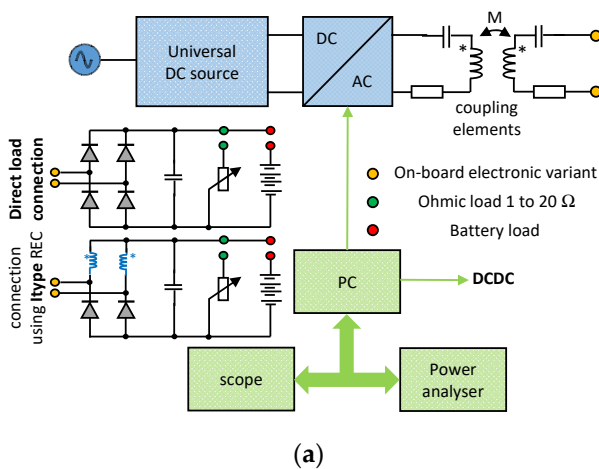


Figure 9. Block diagram of the experimental system setup (a) and physical system setup for testing (b).

A more detailed design regarding the practical realization of the secondary-side rectifier is shown in Figure 10. It is seen that the upper bridge rectifier diodes are replaced

by the inductors, while the values are determined using Equation (22). Consequently, the sizing of the inductor conductor refers to the secondary-side current value.

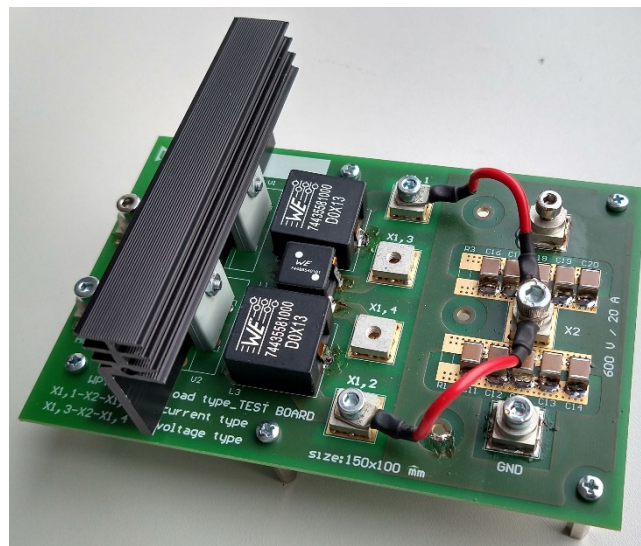


Figure 10. Physical prototype of current-doubler rectifier for investigated WPT system.

The initial experimental verification of the system operation was performed in the form of the analysis of the time waveforms of primary and secondary-side electrical variables. Figure 11 (left) is showing these results for the operation at the optimal value of the load, and Figure 11 (right) shows the operation in a real battery charging application. The measured waveforms in Figure 11 correspond to the simulation results (Figures 7 and 8) in terms of values and shapes.

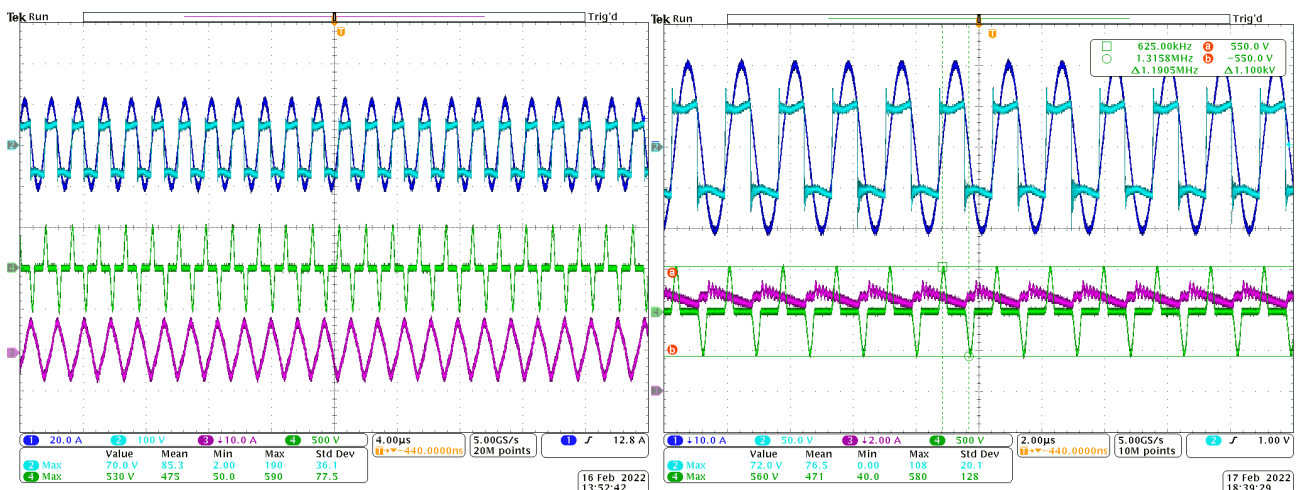


Figure 11. Time waveforms of WPT system with current-doubler rectifier: left for the ideal configuration; right for the real battery charging application (blue—primary current, light blue—primary voltage, left purple—secondary current, right purple—one DC leg current, green—secondary voltage).

Consequently, to perform comparative analysis of the system performance considering various types of the secondary-side rectification, certain modifications regarding system parameters should be performed. With the same supply voltage, the alternative rectifier with a current doubler will deliver much higher power compared to the default system (“A”). There are at least three ways to deal with this. We will mark them with the letters “B”, “C” and “D”.

- Option “B” assumes the preservation of the circuit parameters, and therefore, it is necessary to reduce the supply voltage to the value (23) with the help of (11).
- Option “C” considers the same supply voltage as option “A”, and therefore, a modification of the secondary circuit is necessary. Considering (13), it is enough to recalculate the secondary inductance according to (23).
- Option “D” is a completely new system design with an equivalent load determined by Equation (23).
- The results of all variants are compared in Table 3, where ΔP_{j1} and ΔP_{j2} denote the winding losses on the primary and secondary side.

Table 3. The results of the operational performance of analyzed WPT system.

Parameter	“A”	“B”	“C”	“D”
U_{1DC} (V)	55	25	50	58
L_1 (μ H)	5.5	5.5	5.5	13.323
L_2 (μ H)	5.5	5.5	27.14	13.323
L_{3_L4} (μ H)	N/A	0.97	0.97	0.97
C_1 (nF)	142.12	142.12	142.12	58.68
C_2 (nF)	142.12	142.12	28.8	58.68
C_e (nF)	N/A	162	162	162
R_1 (m Ω)	90	90	90	90
R_2 (m Ω)	90	90	90	90
ΔP_{j1} (W)	3	18.17	3.37	5
ΔP_{j2} (W)	13.77	2.5	4.63	4
P_Z (W)	204.85	201.9	199	205
η (%)	92.27	87	96	91.7

- As can be seen from the results, option “B” comes out as the worst one. The reason is the lower voltage compared to other options and thus the higher losses due to the higher current flowing on the primary side. However, the transfer of the losses from the secondary side to the primary side is favorable here, which can play a significant role in the case of a waterproof design of the charger. Option “D” comes out in terms of overall efficiency like opt. “A”, but its lower THDi (due to the type of the used rectifier) leads to lower apparent power. This has a favorable effect regarding power losses in the primary winding and brings an indisputable advantage from a thermal management point of view. Option “C” is characterized with the best efficiency of all the investigated variations.
- Because the operation of the WPT system is not fixed for one defined value of the load, the sensitivity analysis of options “A” and “C” was performed regarding the load variations. This approach is a key factor, which would determine the selection of the proper topology for WPT charger design.
- From the results (Table 4), it is seen that opt. “A” achieved the maximum efficiency for the $2R_Z$ value, and a constant efficiency decline rate can be observed above the $2R_Z$ operating point. The reason why opt. “A” has achieved the maximum efficiency for different state instead of the nominal, lies in fact that the equivalent load does not have enough value according to (23).

$$\begin{aligned}
 \eta_{MAX(S-S)} &\approx 1 - \frac{2R_1\sqrt{\omega^2 M^2}}{\omega^2 M^2} \approx 1 - \frac{2R_1}{\sqrt{\omega^2 M^2}} \approx \\
 &1 - \frac{2}{k\sqrt{Q_1 Q_2}} \tag{24} \\
 R_{Z-opt(S-S)} &\approx k\omega L \\
 R_Z &\geq R_{Z-opt(S-S)}
 \end{aligned}$$

Therefore, one of the alternative rectifier topology advantages may consist within the condition (24) for easier fulfillment.

Table 4. The results of the operational performance of analyzed WPT system.

	Parameter	R_Z	$2R_Z$	$3R_Z$	$4R_Z$	$5R_Z$
Opt. "A"	P_Z (W)	204.85	394.14	562.22	703.6	834.42
	η (%)	92.27	94.11	93.8	92.68	92.18
Opt. "C"	P_Z (W)	199	380	471.75	517.52	551.21
	η (%)	96	95.61	94.87	94.23	93.56

5. Discussion

The experiments agreement with the simulations, which is shown above in Section 4, alongside a summary of the experimental results. Graphical representation of the experimental results is given in Figure 12 for Table 3 and in Figure 13 for Table 4, showing satisfactory results.

At the beginning, the proposed alternative I-type rectifier consists of only two diodes and two high-quality inductors without mutual coupling, so the lower rectifier power losses are expected as well. This phenomenon is certified by Figure 12, which captures the system efficiency in the optimal load case. Therefore, but not because of that, the proposed solution is advantageous.

Next, according to the construction, the proposed solution is cheaper and smaller than that of a standard diode rectifier and especially than active impedance-matching circuits and, in some cases, than alternative passive impedance matching of the wireless power transfer load.

Finally, the proposed solution shows better properties in real application conditions, too. Figure 13 shows the system efficiency under real conditions—it means under different load values especially.

The proposed solution can increase the system efficiency with low costs, small space and small complications.

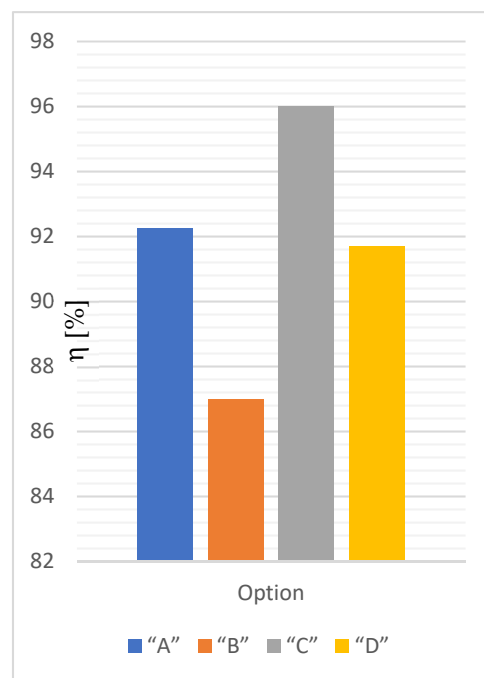


Figure 12. The results of the operational performance of analyzed WPT system—all options in optimal system state.



Figure 13. The results of the operational performance of analyzed WPT system—option A and option C under variable load values.

6. Conclusions

This paper provides a system analysis of the wireless power transfer system equipped with an alternative secondary-side rectifier solution. The proposed solution represents a proper choice for the applications where low equivalent load is presented. An analytical approach was performed in order to find the optimal value of the secondary-side current-doubler inductances—in order to meet the highest possible efficiency for defined operational condition. Several relationships have been discussed during the analysis, thus enabling electrical engineers to understand the design process of certain WPT systems with an alternative topology of the secondary-side rectifier. The experimental verification of the operational performance was realized under laboratory conditions, while the proposed solution was adequately adapted to meet the required input–output parameters of commonly used systems equipped by a standard bridge-voltage rectifier. Mutual comparison from an efficiency point of view is given by laboratory verification—the achieved results show that the presented alternative improves the operational efficiency for nominal parameters by 3.73% (bridge rectifier—92.27%, current-doubler rectifier—96%). A second experiment was performed in the way of load variation sensitivity analysis, whereby the proposed solution exhibits higher efficiency in comparison to the standard solution within the whole operational range. Based on these facts, it is worth saying that for the case of the specific application purpose (low equivalent loads) of the WPT system, the presented solution represents an attractive alternative that is not complex. The future works will be more focused on the EMI performance evaluation of the proposed alternative solution of the secondary-side rectifier of the WPT system. The reasons for this are that from natural operation, it was seen (Figures 7 and 8) that the voltage stress is much higher compared to the standard solutions of the rectifiers. Therefore, the relation between circuit components values (current-doubler inductors) and the possibilities for voltage stress reduction will be performed in greater detail.

Author Contributions: V.K.: investigation, writing—original draft preparation, project administration, methodology, M.Z.: investigation, validation, M.T.: investigation, validation, J.S.: investigation, validation, M.F.: methodology, investigation, writing—review and editing, funding acquisition. All authors have read and agreed to the published version of the manuscript.

Funding: This research has been supported by the funding program of the University of West Bohemia number SGS-2021-021. The authors would like to thank also the Slovak national grant agency VEGA for project support 1/0063/21. This work was also supported by the Ministry of Education, Youth and Sports of the Czech Republic under the project OP VVV Electrical Engineering Technologies with High-Level of Embedded Intelligence CZ.02.1.01/0.0/0.0/18_069/0009855.

Data Availability Statement: Data are contained within the article.

Conflicts of Interest: The authors declare no conflict of interest.

References

1. Rim, C.T. Chapter 34—Wireless Charging of Electric Vehicles. In *Power Electronics Handbook*, 4th ed.; Butterworth-Heinemann: Oxford, UK, 2018; pp. 1113–1137, ISBN 9780128114070. [\[CrossRef\]](#)
2. Van Mulders, J.; Delabie, D.; Lecluyse, C.; Buyle, C.; Callebaut, G.; Van der Perre, L.; De Strycker, L. Wireless Power Transfer: Systems, Circuits, Standards, and Use Cases. *Sensors* **2022**, *22*, 5573. [\[CrossRef\]](#) [\[PubMed\]](#)
3. Tran, M.T.; Thekkan, S.; Polat, H.; Tran, D.-D.; El Baghdadi, M.; Hegazy, O. Inductive Wireless Power Transfer Systems for Low-Voltage and High-Current Electric Mobility Applications: Review and Design Example. *Energies* **2023**, *16*, 2953. [\[CrossRef\]](#)
4. Houran, M.A.; Yang, X.; Chen, W.; Hanif, A.; Hassan, A.; Qin, M. Wireless Power Transfer System for Automatic Revolving Doors. In Proceedings of the 2021 IEEE Energy Conversion Congress and Exposition (ECCE), Vancouver, BC, Canada, 10–14 October 2021; pp. 5851–5855. [\[CrossRef\]](#)
5. Jena, S.; Sahu, P.K.; Mohapatra, S.K. Chapter 19—Efficient wireless power transfer system for biomedical applications. In *Electronic Devices, Circuits, and Systems for Biomedical Applications*; Academic Press: Cambridge, MA, USA, 2021; pp. 405–422, ISBN 9780323851725. [\[CrossRef\]](#)
6. Beeby, S.; Arumugam, S.; Hillier, N.; Li, Y.; Shi, J.; Sun, Y.; Wagih, M.; Yong, S. Chapter 9—Power supply sources for smart textiles. In *The Textile Institute Book Series, Smart Clothes and Wearable Technology*, 2nd ed.; Woodhead Publishing: Cambridge, UK, 2023; pp. 211–236, ISBN 9780128195260. [\[CrossRef\]](#)
7. Wu, X.; Xue, H.; Zhao, S.; Han, J.; Chang, M.; Liu, H.; Li, L. Accurate and Efficient Method for Analyzing the Transfer Efficiency of Metasurface-Based Wireless Power Transfer System. *IEEE Trans. Antennas Propag.* **2023**, *71*, 783–795. [\[CrossRef\]](#)
8. Liu, X.; Wang, T.; Yang, X.; Jin, N.; Tang, H. Analysis and Design of a Wireless Power Transfer System with Dual Active Bridges. *Energies* **2017**, *10*, 1588. [\[CrossRef\]](#)
9. Seshadri, S.; Kavitha, M.; Bobba, P.B. Effect of coil structures on performance of a four-coil WPT powered medical implantable devices. In Proceedings of the 2018 International Conference on Power, Instrumentation, Control and Computing (PICC), Thrissur, India, 18–20 January 2018; pp. 1–6. [\[CrossRef\]](#)
10. Tian, X.; Chau, K.T.; Han, W.; Lee, C.H.T. Design and Analysis of Double-Layer Electromagnetic Field Limiter for Wireless Rechargeable Medical Implants. *IEEE Trans. Magn.* **2021**, *57*, 5100206. [\[CrossRef\]](#)
11. Hong, S.; Jeong, S.; Lee, S.; Sim, B.; Kim, H.; Kim, J. Low EMF Design of Cochlear Implant Wireless Power Transfer System using A Shielding Coil. In Proceedings of the 2020 IEEE International Symposium on Electromagnetic Compatibility & Signal/Power Integrity (EMCSI), Reno, NV, USA, 27–31 July 2020; pp. 623–625. [\[CrossRef\]](#)
12. Kumar, A.; Bertoluzzo, M.; Jha, R.K.; Sagar, A. Analysis of Losses in Two Different Control Approaches for S-S Wireless Power Transfer Systems for Electric Vehicle. *Energies* **2023**, *16*, 1795. [\[CrossRef\]](#)
13. Yamaguchi, M.; Kusaka, K.; Itoh, J.-I. Experimental Loss Separation of Mega-hertz Inverter for WPT System using Calorimetric Power Loss Measurement. In Proceedings of the 2021 IEEE International Future Energy Electronics Conference (IFEEEC), Taipei, Taiwan, 16–19 November 2021; pp. 1–6. [\[CrossRef\]](#)
14. Yu, J.; Ng, W.L.; Xia, M.; Gao, Z. Loss Modelling and Analysis of a High-Efficiency Wireless Power Transfer System for Automated Guided Vehicle Applications. In Proceedings of the 2021 22nd International Conference on Electronic Packaging Technology (ICEPT), Xiamen, China, 11–14 August 2021; pp. 1–6. [\[CrossRef\]](#)
15. Zhu, L.; Jiang, C.; Wang, S. Research on MC-WPT System with Wide Input Voltage Range. In Proceedings of the 2020 8th International Conference on Power Electronics Systems and Applications (PESA), Hong Kong, China, 7–10 December 2020; pp. 1–6. [\[CrossRef\]](#)
16. Liu, Z.; Wang, L.; Guo, Y.; Tao, C. Eddy Current Loss Analysis of Wireless Power Transfer System for Autonomous Underwater Vehicles. In Proceedings of the 2020 IEEE PELS Workshop on Emerging Technologies: Wireless Power Transfer (WoW), Seoul, Republic of Korea, 15–19 November 2020; pp. 283–287. [\[CrossRef\]](#)
17. Cheng, B.; He, L.; Li, L.; Liu, H.; Lu, F. Improved wireless power transfer system utilizing a rectifier with nonlinear resistance compression characteristic. *Appl. Energy* **2023**, *331*, 120365. [\[CrossRef\]](#)
18. Berger, A.; Agostinelli, M.; Vesti, S.; Oliver, J.A.; Cobos, J.A.; Huemer, M. A Wireless Charging System Applying Phase-Shift and Amplitude Control to Maximize Efficiency and Extractable Power. *IEEE Trans. Power Electron.* **2015**, *30*, 6338–6348. [\[CrossRef\]](#)
19. Lang, H.-D.; Ludwig, A.; Sarris, C.D. Maximum transfer efficiency and optimal loads for WPT systems with multiple transmitters. In Proceedings of the 2014 IEEE Antennas and Propagation Society International Symposium (APSURSI), Memphis, TN, USA, 6–12 July 2014; pp. 430–431. [\[CrossRef\]](#)

20. Duong, Q.-T.; Okada, M. Maximum efficiency formulation for inductive power transfer with multiple receivers. *IEICE Electron. Express* **2016**, *13*, 20160915. [CrossRef]
21. Fu, M.; Yin, H.; Zhu, X.; Ma, C. Analysis and Tracking of Optimal Load in Wireless Power Transfer Systems. *IEEE Trans. Power Electron.* **2015**, *30*, 3952–3963. [CrossRef]
22. Zhong, W.; Hui, S.Y.R. Maximum Energy Efficiency Operation of Series-Series Resonant Wireless Power Transfer Systems Using On-Off Keying Modulation. *IEEE Trans. Power Electron.* **2018**, *33*, 3595–3603. [CrossRef]
23. Zhang, J.; Wang, F. Efficiency Analysis of Multiple-Transmitter Wireless Power Transfer Systems. *Int. J. Antennas Propag.* **2018**, *2018*, 3415239. [CrossRef]
24. Yang, D.; Won, S.; Tian, J.; Cheng, Z.; Kim, J. A Method of Estimating Mutual Inductance and Load Resistance Using Harmonic Components in Wireless Power Transfer System. *Energies* **2019**, *12*, 2728. [CrossRef]
25. Ahn, D.; Kim, S.; Moon, J.; Cho, I.-K. Wireless Power Transfer with Automatic Feedback Control of Load Resistance Transformation. *IEEE Trans. Power Electron.* **2016**, *31*, 7876–7886. [CrossRef]
26. Adewuyi, V.O. Overview and Advancements in Electric Vehicle WPT Systems Architecture. In *Power Electronics, RF, and Microwave Engineering* [Working Title]. 2022. Available online: <https://www.intechopen.com/online-first/84947> (accessed on 6 November 2023). [CrossRef]
27. Ahire, D.B.; Gond, V.J.; Chopade, J.J. Compensation topologies for wireless power transmission system in medical implant applications: A review. *Biosens. Bioelectron. X* **2022**, *11*, 100180. [CrossRef]
28. Haruna, J.; Kavimandan, U.D.; Onar, O.; Galigekere, V.P.; Pries, J. Sensitivity Analysis of Compensation Topologies for Dynamic WPT System. In *Proceedings of the 2020 IEEE Transportation Electrification Conference & Expo (ITEC)*, Chicago, IL, USA, 19–21 June 2020; pp. 284–289. [CrossRef]
29. Yi, W.; Ming, L.; Zhongping, Y.; Fei, L. Analysis and Comparison of SP and S/SP Compensated Wireless Power Transfer System for AGV Charging. In *Proceedings of the 2020 IEEE 3rd International Conference on Electronics Technology (ICET)*, Chengdu, China, 8–11 May 2020; pp. 485–488. [CrossRef]
30. Zhang, W.; Mi, C.C. Compensation Topologies of High-Power Wireless Power Transfer Systems. *IEEE Trans. Veh. Technol.* **2016**, *65*, 4768–4778. [CrossRef]
31. Mude, K.N.; Aditya, K. Comprehensive review and analysis of two-element resonant compensation topologies for wireless inductive power transfer systems. *Chin. J. Electr. Eng.* **2019**, *5*, 14–31. [CrossRef]
32. Dai, X.; Li, X.; Li, Y.; Hu, A.P. Impedance-matching range extension method for maximum power transfer tracking in IPT System. *IEEE Trans. Power Electron.* **2018**, *33*, 4419–4428. [CrossRef]
33. Zhang, Y.; Li, X.; Chen, S.; Tang, Y.I. Soft switching for strongly coupled wireless power transfer system With 90° dual-side phase shift. *IEEE Trans. Ind. Electron.* **2022**, *69*, 282–292. [CrossRef]
34. Guan, Y.; Bian, Q.; Wang, Y.; Hu, X.; Liu, B.; Wang, W.; Xu, D. Analysis and design of high-frequency converter with resistive matching network and spiral inductor. *IEEE Trans. Power Electron.* **2018**, *33*, 5062–5075. [CrossRef]
35. Zhang, K.; Gao, W.; Shi, R.; Yan, Z.; Song, B.; Hu, A.P. An impedance matching network tuning method for constant current output under mutual inductance and load variation of IPT System. *IEEE Trans. Power Electron.* **2020**, *35*, 11108–11118. [CrossRef]
36. Seo, D.-W.; Lee, J.-H.; Lee, H.-S. Optimal Coupling to Achieve Maximum Output Power in a WPT System. *IEEE Trans. Power Electron.* **2016**, *31*, 3994–3998. [CrossRef]
37. Park, C.-B.; Lee, H.-W. Study on the optimal switching frequency for maximum wireless power transfer in a variable airgap system. *IEEE Trans. Emerg. Sel. Top. Power Electron.* **2015**, *3*, 201–204. [CrossRef]
38. Su, M.; Liu, Z.; Zhu, Q.I.; Hu, A.P. Study of maximum power delivery to movable device in omnidirectional wireless power transfer system. *IEEE Access* **2018**, *6*, 76153–76164. [CrossRef]
39. Dai, X.; Li, X.; Li, Y.; Hu, A.P. Maximum efficiency tracking for wireless power transfer systems with dynamic coupling coefficient estimation. *IEEE Trans. Power Electron.* **2018**, *33*, 5005–5015. [CrossRef]
40. Miao, Z.; Liu, D.; Gong, C. Efficiency enhancement for an inductive wireless power transfer system by optimizing the impedance matching networks. *IEEE Trans. Biomed. Circuits Syst.* **2017**, *11*, 1160–1170. [CrossRef]
41. Kindl, V.; Frivaldsky, M.; Zavrrel, M.; Pavelek, M. Generalized Design Approach on Industrial Wireless Chargers. *Energies* **2020**, *13*, 2697. [CrossRef]
42. Detka, K.; Górecki, K. Wireless Power Transfer—A Review. *Energies* **2022**, *15*, 7236. [CrossRef]
43. Lin, Y.; Zhao, Z. Topology and control strategy on transformerless wireless power station for future electric transportation systems. *Int. Trans. Electr. Energ. Syst.* **2021**, *31*, e13019. [CrossRef]
44. Li, J.; Wang, J.; Wang, P.; Li, J.; Chen, J.; Chen, S. Design and Control of a Three-Level Rectifier in LCC/S-Compensated IPT for Wide Output Voltage Regulation over Various Magnetic Couplings. *Electronics* **2022**, *11*, 1426. [CrossRef]
45. Zou, S.; Onar, O.C.; Galigekere, V.; Pries, J.; Su, G.-J.; Khaligh, A. Secondary Active Rectifier Control Scheme for a Wireless Power Transfer System with Double-Sided LCC Compensation Topology. In *Proceedings of the IECON 2018—44th Annual Conference of the IEEE Industrial Electronics Society*, Washington, DC, USA, 21–23 October 2018; pp. 2145–2150. [CrossRef]

Disclaimer/Publisher’s Note: The statements, opinions and data contained in all publications are solely those of the individual author(s) and contributor(s) and not of MDPI and/or the editor(s). MDPI and/or the editor(s) disclaim responsibility for any injury to people or property resulting from any ideas, methods, instructions or products referred to in the content.